J Appl Electrochem (2008) 38:395–402
DOI 10.1007/s10800-007-9450-x

ORIGINAL PAPER

Sonoelectrochemical (20 kHz) production of $Co_{65}Fe_{35}$ alloy nanoparticles from Aotani solutions

M. Dabalà · B. G. Pollet · V. Zin · E. Campadello · T. J. Mason

Received: 15 June 2007 / Revised: 9 November 2007 / Accepted: 9 November 2007 / Published online: 22 November 2007

Abstract This paper describes the production of alloy nanoparticles of Co:Fe ratio 65:35 from Aotani solutions in the presence of high power ultrasound (20 kHz). The production of this new type of alloy nanoparticles was performed potentiostatically and galvanostatically at (298 ± 1) K using a newly designed experimental set-up i.e. a 'sonoelectrode' producing short applied current pulses triggered and followed immediately by ultrasonic pulses. It was shown that cathode efficiencies decreased with increasing current densities and high nanoparticle yields were obtained at low current densities. Morphological and structural studies of the produced nanoparticles were performed by TEM, SEM, XRD, and SAED, and showed that the strongly aggregated $Co_{65}Fe_{35}$ alloy nanoparticles were predominantly formed, with prevalent body-centered cubic *bcc* crystalline structure; no redissolution of the nanoaggregates was observed and no separate Fe and Co metallic nanoparticles were produced sonoelectrochemically. The experimental value of the lattice parameter for *bcc* Co–Fe alloy was 2.85 Å and was in excellent agreement with literature values.

M. Dabalà · V. Zin · E. Campadello
DIMEG—University of Padua, via Marzolo, 9, 35131 Padova, Italy

B. G. Pollet (✉)
Fuel Cells Group, Chemical Engineering Department, The University of Birmingham, Edgbaston Road, Birmingham B15 2TT, UK
e-mail: b.g.pollet@bham.ac.uk

T. J. Mason
Faculty of Health and Life Sciences, Coventry University, Priory Street, Coventry CV1 5FB, UK

Keywords Sonochemistry · Electrochemistry · Nanoparticles · Power ultrasound

1 Introduction

The effect of high power ultrasound on electrochemical systems or Sonoelectrochemistry is an active and exciting research area. It was shown that the effects of high intensity ultrasonic irradiation on electrochemical processes lead to both chemical and physical effects, for example, mass-transport enhancement, surface cleaning and radical formation. Many workers [1–4] have also investigated the distribution of ultrasonic waves or energy in various electrochemical reactors operating in the lower ultrasonic frequency range (20–55 kHz) and at high ultrasonic powers. Several methods for such determination have been proposed e.g. aluminum foil erosion, sonoluminescence, calorimetric methods, chemical dosimetry and laser-sheet visualization [1–4].

Many of the observed effects in Sonoelectrochemistry may be explained by the enhancement of mass-transport in diffusion-controlled processes [4]. Low-frequency high power ultrasound is known to decrease the diffusion layer thickness (δ) thereby giving substantial increase in limiting current (I_{lim}) attributed due to effects of cavitation and/or micro and macro-streaming [3, 4]. The experimental decrease in the diffusion layer thickness is also known to be due to asymmetrical collapse of cavitation bubbles at the electrode surface leading to the formation of high velocity jets of liquid being directed toward its surface. This jetting, together with acoustic streaming, is thought to lead to random punctuation and disruption of the mass transfer boundary layer at the electrode surface at close electrode-to-horn separations. More recently, Pollet et al. [5] showed,

with aid of mathematical models based on mass-balance equations, that a Levich-like equation relating the limiting current density, the square root of ultrasonic intensity and the inverse square root of the electrode-horn distance, may be generated for ultrasonic frequencies of 20 and 40 kHz allowing the generation of an 'equivalent' flow velocity under sonication, an important and useful parameter in chemical engineering.

Due to the numerous advantages of Sonoelectrochemistry, recently, an upsurge of interests has been observed in the synthesis of metallic nanoparticles [6–9].

In the last decade, the production of metallic cobalt–iron alloys nanoparticles has been investigated as they offer high surface-to-volume ratios and have considerable potential for usage in various areas e.g. magnetic recording, catalysis, and medicine [10–16]. There are a range of methods of producing metallic nano-sized materials including thermal decomposition [17, 18], physical and thermal evaporation [6, 17], laser ablation [19], laser-assisted catalytic growth (LCG) [11, 12], vapor–liquid–solid growth (VLS) [11], chemical oxidation [12] and sol–gel methods [13]. However most of these techniques tend to be expensive and time-consuming. An alternative method, which is both simple and cost-effective, is the use of Sonoelectrochemistry. For example, Reisse et al. [14] produced micro sized metallic particles such as copper by a unique sonoelectrochemical method, in which the ultrasonic horn was used as the working electrode. This 'sonotrode' or 'sonoelectrode' was subjected to short applied current pulses which were each followed by ultrasonic pulses. They showed that, during cavitation, a jet of liquid penetrates inside the cavitation bubble perpendicular to the 'sonoelectrode' surface [16] and the resulting impact was responsible for dislodging any nanopowder material which had been electrochemically deposited on the surface. This new sonoelectrochemical method has since been employed to produce several pure metallic, alloy [14, 20–22] and semiconductor nanoparticles [23–26].

This paper presents a study on the synthesis of cobalt–iron alloys nanoparticles using the new method combining metallic electrodeposition with power ultrasound (20 kHz). The cobalt–iron alloys nanopowders produced were characterized both morphologically and chemically.

2 Experimental

The experiments were carried out in two stages:

(i) Potentiostatic and galvanodynamic characterization of the electrochemical behaviour of the Aotani solution in the absence and presence of ultrasound, and
(ii) Synthesis by electrolysis and characterization of produced cobalt–iron alloys nanoparticles were performed by using the pulsed sonoelectrochemical method [14].

For the first stage of this investigation, all electrochemical experiments were performed either potentiostatically or galvanostatically using either a Radiometer PGP201 potentiostat or a AMEL 7060 potentiostat respectively connected to a PC for data acquisition. Electrochemical experiments were performed using either a cell similar design to that of Pollet et al. [27] (Fig. 1a) or in a cylindrical vessel (200 ml) (Fig. 1b). Electrochemical cells were placed in a Faraday cage. Temperature was regulated by a glass cooling coil (C) placed inside the electrochemical cell and linked to a thermostatted bath operating at

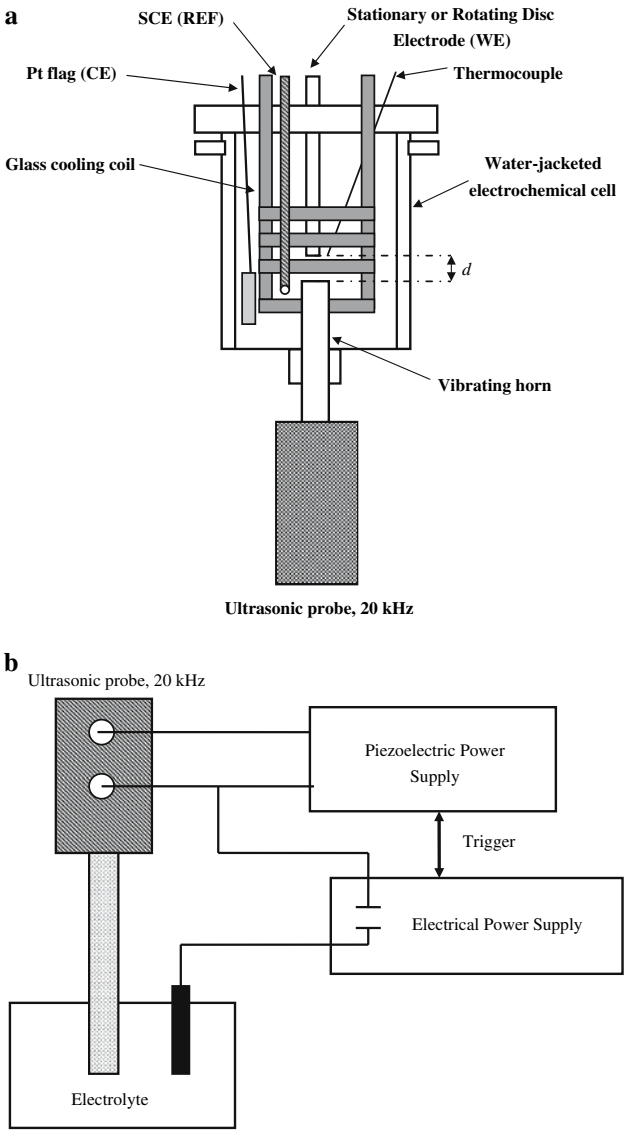

Fig. 1 (**a**) The *Pollet* arrangement [27] with the exception of the ultrasonic source (20 kHz Vibra-Cell VC600 probe) at the bottom; (**b**) Schematic of the sonoelectrochemical nanoparticle production setup

preset temperatures. The temperature of the electro-analyte was measured with a Fluke 51 digital thermometer fitted to a K-type thermocouple. The working electrodes were either a titanium disc (r = 0.066 cm, area = 0.0136 cm^2 determined coulometrically) for the 'face-on' mode [27] (Fig. 1a) or a titanium alloy sonoelectrode (r = 0.625 cm, area = 1.227 cm^2) (Fig. 1b).

Platinum flags and meshes were used as counter electrodes. For potentiostatic studies, the distance between the ultrasonic probe and the working electrode was (2 ± 0.1) mm (d, Fig. 1a) and for galvanostatic studies, the ultrasonic horn was used as the working electrode (Fig. 1b). All electrodes were electrochemically cleaned by cycling in sulphuric acid (1.0 mol dm^{-3}) for 10 min prior to the experiments. They were then washed with high quality MilliQ water and all Ti electrodes were polished to a mirror finish first with grinding paper (Buelher-Met, P600) and then sequentially with 25 microns down to 0.3 micron alumina oxide paste. For potentiostatic studies, a saturated calomel electrode (sce) was employed as reference electrode.

For the second stage of this study, the apparatus employed for the production of cobalt–iron alloy nanosized materials was similar to that employed by Reisse et al. [14]. The system consisted of a two-electrode set-up, namely (i) a titanium alloy horn (Sonics & Materials) acting both as the cathode and the ultrasonic emitter (described therein as the 'sonoelectrode') linked to a AMEL 7060 potentiostat operating in galvanostatic mode and a 20 kHz Ultrasonic VC-600 Sonics & Materials generator and (ii) a platinum mesh acting as the anode linked to the potentiostat. A heat-shrinkable sleeve surrounded the side walls of the extreme part of the sonoelectrode, leaving only a flat active surface for the electrodeposition equal to 1.227 cm^2 (ultrasonic horn tip area determined coulometrically) (Fig. 1b). A constant galvanostatic current was applied to the sonoelectrode and the maximum ultrasonic power ultrasound employed was 76 W. A trigger acted like a switch with the role of closing alternatively the circuits in which the potentiostat and the piezoelectric power supply operated. The pulse drivers allowed applied galvanic current and ultrasonic pulsing.

For the production of nanopowders, the time management sequence employed was as follows:

(1) A short current pulse was sent to the sonoelectrode, and here the titanium horn acts as an electrode only (t_{ON}); the time of this phase typically ranged between 0.3 and 0.5 s.
(2) Immediately after the electrochemical pulse was turned off, an ultrasonic pulse was sent to the sonoelectrode and here it acted only as a vibrating ultrasonic horn (t_{US}); this second phase lasts no more than 0.5 s
(3) A rest time, t_p, followed the two previous phases (this was useful to restore the initial electrolyte conditions close to the sonoelectrode).

A characteristic time management parameter of the process, χ, was employed according to Eq. 1 [14]:

$$\chi = \frac{t_{ON}}{t_{ON} + t_{OFF}} \tag{1}$$

where $t_{OFF} = t_{US} + t_p$.

By controlling the varying process parameter, χ, and the applied current, it was possible to produce sonoelectrochemically high purity and high surface/volume ratio suspended nanoparticles which were filtered with 0.05 μm Millipore filters under vacuum.

The filters were then washed with pure ethanol, dried for 48 h in a silica-gel drier and stored under vacuum. Each filter was weighted after dehydration and the efficiency of the process was calculated as the ratio of the produced mass of powder to the faradic yield according to Eq. 2 [28]:

$$m_f = \frac{\chi \cdot I \cdot t}{F} \cdot \frac{\sum_i (x_i \cdot PA_i)}{\sum_i (x_i \cdot n_{ei})} \tag{2}$$

where χ is $t_{ON}/(t_{ON} + t_{OFF})$, I is the applied current in A, t is the total time in s, F is the Faraday constant (96,500 C mol^{-1}), x_i is the molar fraction, PA_i is the atomic weight in g mol^{-1} and n_{ei} is the number of electron transferred.

For each run, the cathode efficiency, η in % was determined using Eq. 3 [29]:

$$\eta = \frac{m_r}{m_f} \cdot 100\% \tag{3}$$

where m_f is the faradaic yield in g and m_r is the actual metallic mass produced during the sonoelectrochemical tests in g.

The formed powders were analyzed by X-ray fluorescence (Kevex Analyst 770) in views of identifying their exact chemical composition. Morphological studies of the nanopowders were performed on both a scanning electron microscope, SEM (Stereoscan 440 SEM, Cambridge, equipped with a Philips EDAX PV9800) and a transmission electron microscope, TEM (JEOL 3010 operating at 300 kV). X-ray diffractometer (Siemens D500 XRD) with CuK_α radiation [λ(Cu) = 1.54060 Å] was used for the identification of the phases and the measurement of grain size in the powders.

Finally, for all experiments, chemical reagents were of AnalaR grade or equivalent. All $Co_{65}Fe_{35}$ nanopowders were synthesized from a sulphate bath based on Aotani's formulation [30] and its composition is shown in Table 1. The pH was adjusted to ca. 3 with a 6.0 mol dm^{-3} solution of HCl and the solution was exposed to air [31]. Citric acid (weak organic acid) was used as a buffer to increase

Table 1 Composition of $Co_{65}Fe_{35}$ Aotani's bath

Chemicals for Aotani's bath	Concentration/mol dm^{-3}
$FeSO_4 \cdot 7H_2O$	0.0945
$CoSO_4 \cdot 7H_2O$	0.1755
NH_4Cl	0.48
H_3BO_3	0.48
$C_6H_8O_7$	0.01
NaOH	0.017

'solubility'. Aqueous Aotani's solutions were prepared using high quality MilliQ water (R = 12 MΩ). Ultrasonic powers were determined calorimetrically using the method of Margulis et al. [32, 33] and ultrasonic powers are quoted as W or otherwise stated.

3 Results and discussion

3.1 Potentiostatic studies in the absence and presence of Ultrasound (20 kHz)

Potentiostatic experiments were performed using a titanium rotating disc electrode in the absence and presence of ultrasound in order to understand the electro-reduction processes involved in the cobalt and iron in solutions. The experimental set-up used is shown in Fig. 1a.

3.1.1 Silent conditions

The electrochemical behavior of the Co–Fe in Aotani's solution was first investigated using cyclic voltammetry on a static Ti disc electrode at 200 mV s^{-1} and at (298 ± 1) K. The scan potential range was run from open circuit potential and always initiated in the negative direction.

Figure 2 shows a typical cyclic voltammogram obtained under silent conditions in the potential range [+1.0 V; −1.5 V vs. sce]. A current loop in the cathodic branch of the voltammogram is obtained, indicating the three-dimensional (3D) nucleation of Co–Fe and subsequent grain growth [34]. In the cathodic part of the voltammogram the electro-reduction of Co–Fe, i.e. the formation of the binary Co–Fe alloy on Ti, starts at a discharge potential of −0.9 V vs. sce. This observation is in good agreement with literature [34]. In the anodic part of the voltammogram and in the potential range of [−0.5 V; +0.5 V vs. sce], the anodic peak potential on Ti, corresponding to the stripping of Co–Fe, is $E_{pa,Ti}$ = +80 mV vs. sce can be seen. Furthermore, in the potential range studied, the separate discharge of Co and Fe ions were observed.

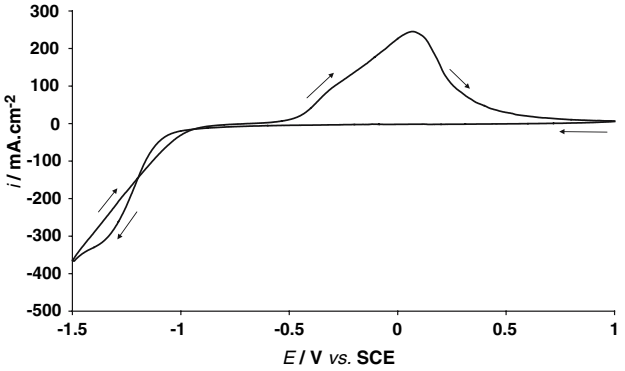

Fig. 2 Cyclic voltammogram of Aotani solution on Ti electrode at 200 mV s^{-1} and at (298 ± 1) K in the absence of ultrasound

The investigation then turned to the effect of forced convection in the absence of ultrasound by using a rotating Ti disc electrode. Figure 3 shows cyclic voltammograms of Ti in Aotani solution at various rotation speeds (up to 1,000 rpm), at 200 mV s^{-1} and at (298 ± 1) K.

The figure shows typical irreversible cyclic voltammograms. In the potential range [+1.0 V; −1.5 V vs. sce], all voltammograms performed at several rotation speeds showed current loops (in the cathodic branches), again, indicating the three-dimensional (3D) nucleation of Co–Fe and subsequent grain growth [34]. In the cathodic part of the voltammograms no limiting currents were observed, indicating that the electro-reduction process of the binary Co–Fe alloy is not only diffusion-controlled but also kinetically-controlled. In the anodic part of the voltammograms, as the rotation speed increased, an increase in anodic peak currents was observed. Furthermore, a negative shift of peak potentials compared to no rotation was observed. For example, a ΔE of −75 mV was obtained at all rotation speeds employed compared with no rotation. This is an interesting observation which could be due to

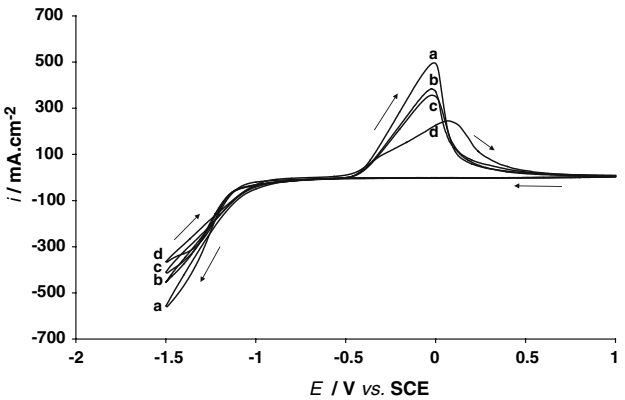

Fig. 3 Series of cyclic voltammograms of Aotani solution on Ti RDE at various rotation speeds (**a**) 1,000 rpm, (**b**) 500 rpm, (**c**) 250 rpm (**d**) 0 rpm, +1.0 V vs. sce to −1.5 V vs. sce, at 200 mV s^{-1}, at (298 ± 1) K in the absence of ultrasound

concentration overpotentials, i.e., as the rate of the electro-reduction reaction is proportional to the surface concentration of the electro-active species, the cathodic reaction rate is limited by a drop in the surface concentration.

3.1.2 *Ultrasonic conditions*

Figure 4 shows typical cyclic voltammograms obtained in the optimized Aotani solution in the absence (dotted line) and presence of ultrasound at 20 kHz and at 118 W cm^{-2} (solid line). For both conditions and in the potential range [+1.0 V; −1.5 V vs. sce], there still exist current loops in the cathodic branch of the voltammograms, indicating nucleation of Fe–Co and grain growth. Also, in this potential range, in the presence of ultrasound, the electro-reduction process for the binary Co–Fe (or discharge potential) starts earlier compared with silent conditions. In other words, there is a potential shift to more positive values (ΔE = +60 mV), a finding that has been observed previously by Pollet et al. [27]. In the potential range [−0.5 V; +0.2 V vs. sce], the anodic response corresponds to the stripping of Co–Fe in the absence and presence of ultrasound. Interestingly, the oxidation (anodic) peak potential is shifted to more negative values (ΔE = −155 mV) in the presence of ultrasound compared to silent conditions.

It is possible to explain this shift in potential as follows:

(a) It is known that when ultrasound is transmitted through a liquid, efficient stirring and cavitation occur in the bulk solution and near the electrode surface [1–4]. This leads to an increase in the movement of ions across the diffusion layer and their subsequent discharge and hence a decrease in concentration overpotential. This also leads to a decrease in nucleation overpotential. It has been shown that ultrasound affects the surface morphology of many metal electrodeposits due to highly efficient stirring caused by acoustic streaming, and also that this decrease in overpotential is due to formation of nucleation sites at the electrode surface caused by the implosion of cavitation bubbles [27].

(b) It is also known that increasing the effective area of an electrode surface causes a decrease in overpotential as is shown by a comparison of typical values for smooth platinum and finely divided platinum black electrodes. Since ultrasound is known to cause pitting of metal surfaces, this is a possible explanation for the decrease in overpotential [27].

(c) Temperature has an obvious influence on electrode kinetics and the potential E is known to be temperature-dependent. Since ultrasonic irradiation can lead to a temperature increase in a medium, it is important to establish whether any observed decrease in potential under sonication is simply due to an increase in bulk temperature. However, in these experiments the temperature of the bulk solution was controlled and never rose above (298 ± 1) K during the sonoelectrochemical runs.

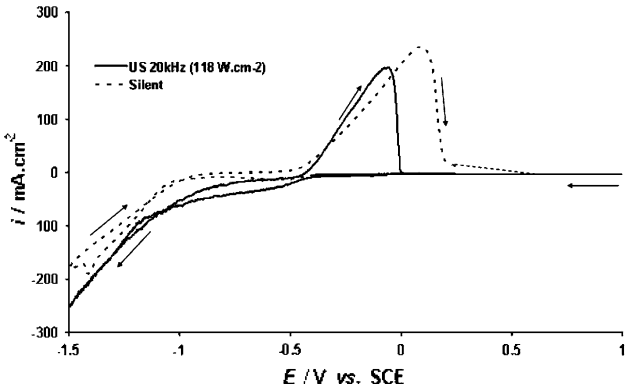

Fig. 4 Cyclic voltammograms of Aotani solution on Ti RDE in the absence (dotted line) and presence of ultrasound (solid line) [20 kHz and 118 W cm^{-2}], at 200 mV s^{-1} and at (298 ± 1) K

3.2 Galvanodynamic studies under silent conditions

The main focus of this study was to determine a value of a 'limiting current' for the system in order to operate under pure "diffusion control" conditions. Under these conditions the overall rate of the reaction is controlled by the rate of the diffusion of the reactants to the electrode surface rather than the rate of the reaction itself. The galvanodynamic experiments were performed with a view to identifying the electrochemical features of the electrolytic solution and to determine the value of the 'limiting current'. A current scan from 0 to −20 mA (scan rate = 0.1 mA s^{-1}) was performed and the cell voltage was monitored. A two electrode configuration was used and the potentiostat was operated in galvanostatic mode.

Figure 5 shows the dependence of cell voltage with the applied current on three electrolytic solutions, containing Fe, Co and $Co_{65}Fe_{35}$. The discharge of 100% Fe and 100% Co start at discharge cell voltages of 1.2 V (Fe) and 2 V (Co). However, the Co:Fe ratio 65:35 curve exhibits two voltage drops (1.5 V and 2 V) which are though to be directly related to the various electro-reduction processes involved. One explanation for this observation is that each voltage drop corresponds to the diffusional processes of Fe^{2+} and Co^{2+}. If the process is performed with lower values of applied current, secondary reactions are inhibited as the process conditions are near the 'limiting current' conditions for the reduction of Fe^{2+} and Co^{2+}.

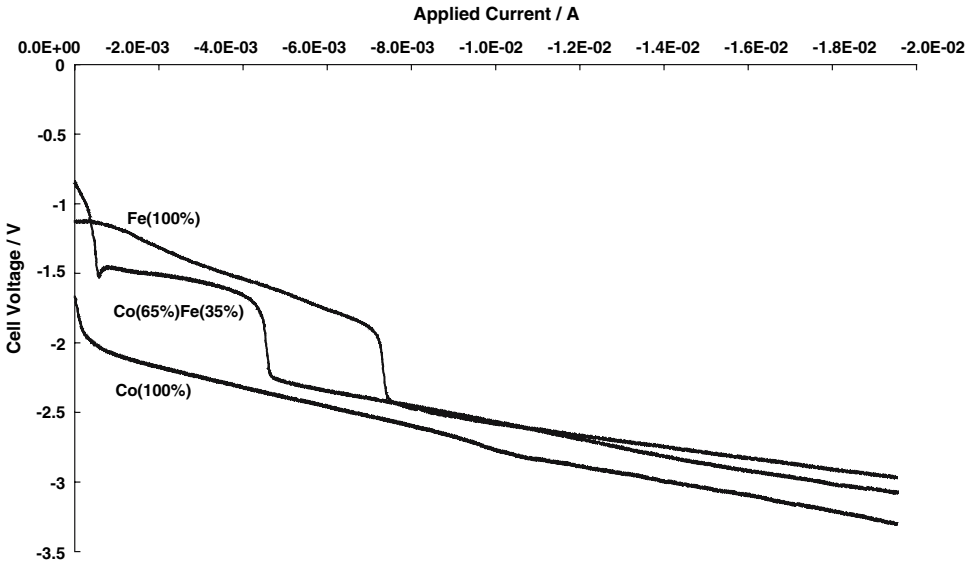

Fig. 5 Galvanodynamic polarisation curves of Fe_{35}, Co_{65}, and $Co_{65}Fe_{35}$ solutions at a scan rate of 0.1 mA s^{-1} and in the range 0 to −20 mA and at (298 ± 1) K

Under such conditions, the highest rate for the charge-transfer reaction compatible with the rate of the diffusion of the cations to the electrode surface is obtained. If however, the applied current is increased the reaction becomes affected by side-reactions as the diffusional process itself is unable to supply the reactants fast enough at the cathode surface.

3.3 Cobalt–iron alloy nanoparticle production

In order to study the system behaviour and to optimize the sonoelectrochemical process, the Co–Fe nanoparticles syntheses were conducted by varying (a) the time duration of t_{ON} and t_{US} between 0.3 and 0.5 s and (b) the applied current from −10 to −500 mA with t_{ON} and t_{US} fixed to 0.3 s as shown in Table 2. The total time of the sono-electrochemical runs was set to 90 min. In these experiments the pH did not significantly vary from the initial value of 3 and no titanium particles arising from cavitational erosion from the ultrasonic horn surface were detected on the filters.

The experimental conditions for the sonoelectrochemical investigations, the process time management parameter, χ and the cathode efficiency, η are summarised in Table 2 from which the following comments can be made:

(a) The cathode efficiency was high and remained over 50% for applied currents lower than −20 mA but as the applied current increased by 50-fold, the cathode efficiency decreased 10-fold. This can be explained as being due to hydrogen evolution which occurs at higher applied currents and therefore cathodic potentials. The electro-reduction of water, as evidenced by hydrogen evolution, is a well-known and undesirable secondary reaction in the metal electrodeposition industry and is the main cause of low cathode efficiencies [29]. From galvanodynamic studies (Fig. 5) and XRF results (not shown here), the optimum applied current window was found to be between −10 and −50 mA.

(b) Variations of t_{ON} and t_{US} influenced the cathode efficiency, particularly for longer ultrasonic and current pulses. For example, at an applied current of −10 mA with t_{ON} = 0.3 s and t_{US} = 0.3 and 0.5 s, it was found that the cathode efficiency decreased from 89% to 52% suggesting that longer ultrasonic pulses were detrimental to the formation of Co–Fe in the bulk electrolyte.

Table 2 Cathode efficiencies (η) showing variation of t_{ON}, t_{US} and applied currents (I)

Tests	I/mA	t_{ON}/s	t_{US}/s	t_p/s	χ	m_t/mg	m_r/mg	η (%)
1	−10	0.3	0.3	0.4	0.33	4.7	4.2	89.0
2	−10	0.5	0.3	0.4	0.47	6.7	5.42	81.0
3	−10	0.3	0.5	0.4	0.25	3.86	2.0	52.0
4	−20	0.3	0.3	0.4	0.33	9.5	5.1	53.7
5	−50	0.3	0.3	0.4	0.33	23.4	2.5	11.0
6	−500	0.3	0.3	0.4	0.33	23.3	19.8	8.5

I is the applied current (mA); t_{ON} is the applied current pulse time (s); t_{US} is the applied ultrasonic pulse time (s); t_p is the rest time (s); χ is the varying process parameter; m_f is the faradic yield (mg); m_r is the actual yield (mg); η is the cathode efficiency (%)

The primary role of ultrasound in these processes is to induce cavitation in the electrolytic solution which will then ablate the metallic nuclei formed during the short electrodeposition period from the cathodic surface [14, 16, 21–26].

The characterization and analyses of nanometallic powders in the filters proved interesting and revealed that their chemical composition was similar to that of the Aotani's solution when the sonoelectrochemical system operated under 'diffusion control', as showed from EDAX (Fig. 6a) and XRF analyses. Furthermore, compositional analysis performed on all filters gave similar results (Table 3); and confirmed that the preferential deposition of the less noble cobalt [35, 36] was not observed, since the electrochemical deposition operated under 'diffusion control'. In fact, the charge of iron and cobalt ions and respective masses were quite similar and so their transport numbers was the same for both species. For this reason the composition of nanoparticles was approximately similar to that of the solution. This is in agreement with the galvanodynamic studies performed previously.

Morphological and structural studies on filters performed by TEM, SEM, XRD, and SAED showed that nanoparticles had prevalent *bcc* crystalline structure and were strongly aggregated (Fig. 6b). TEM images shown in Fig. 6b made possible to observe the smallest particles synthesized with the method, with a minimum size of about 5 nm. However the particles presented a wide size distribution and it was therefore difficult to determine their average size. Furthermore, the nanoparticles produced in this process were agglomerated in clusters and formed three-dimensional structures with mean sizes of about 300 nm with a round shape and which in turn, aggregated and built complex structures, as shown in SEM images (Fig. 6c).

From our findings, it appears that it is not straight-forward to separate individual Co–Fe alloy nanoparticles due to both their magnetic properties [34] and their physical nature, i.e. the high surface energy that leads to aggregation (in order to minimize system energy). The results obtained suggested that the sonoelectrochemical synthesis generated an alloy. Thus, XRD measurements were carried out as shown in Fig. 7 with a view to investigating the microstructure of Co–Fe nanoparticles. The grain size was calculated from the peak broadening using the Rietveld method [37]. The patterns revealed that ca. 93% of Co–Fe nanoparticles produced had a *bcc* structure with lattice parameter of 2.849 Å and an average grain size of ca.12 nm. This is in excellent agreement with the Fe–Co phase diagram according to which the *bcc* phase is thermodynamically stable at temperatures below 1,273 K and the calculated lattice parameter is 2.85 Å [38]. This finding suggests that high pressures and temperatures induced by cavitation, did not appear to influence the crystalline structure of the nanoparticles. Also, no iron oxides were observed in the X-ray diffraction patterns; probably due to the limitation of the technique (i.e. below the detection limit).

Table 3 Results of XRF analyses [Fe(K) and Co(K) lines] showing composition of Fe and Co on all nanometallic powders (filters) using a bath composition of 35% Fe and 65% Co

Tests	%Fe	%Co
1	34.9	65.1
2	43.34	56.66
3	38.82	61.18
4	37.07	62.93
5	35.51	64.49
6	32.78	67.22
Bath composition	35	65

Peak integral method was used

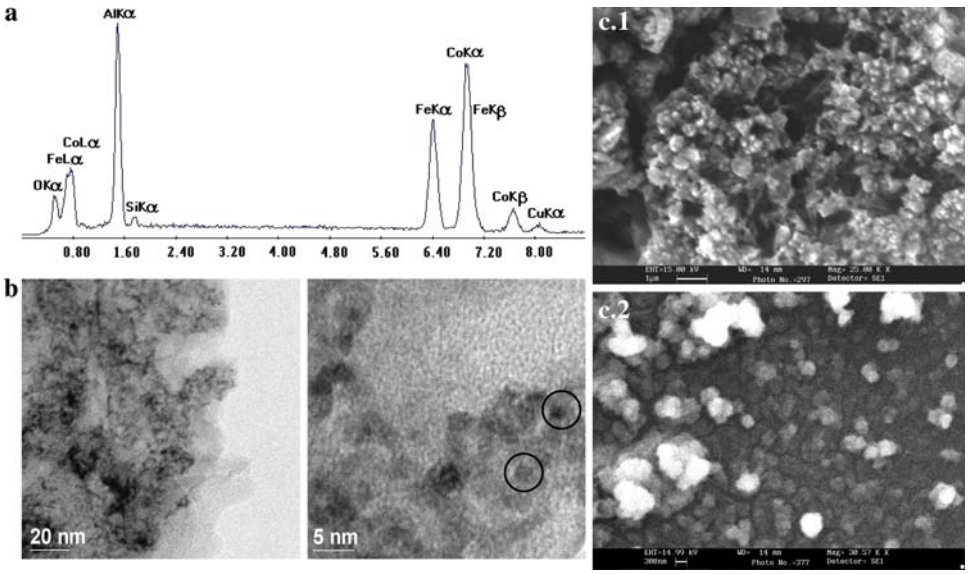

Fig. 6 (**a**) EDAX pattern—Al and Cu peaks originate from the sample holder (made of Al–Cu alloy); Si peak is due to the grinding paper employed to smooth the sample holder; O peak is due to the solvent (the sample holders were thoroughly washed in ethanol and then sonicated); (**b**) TEM images; (**c**) SEM images [specimens prepared by drop-(c.1) casting and (c.2) gilding techniques] of Co–Fe nanopowders

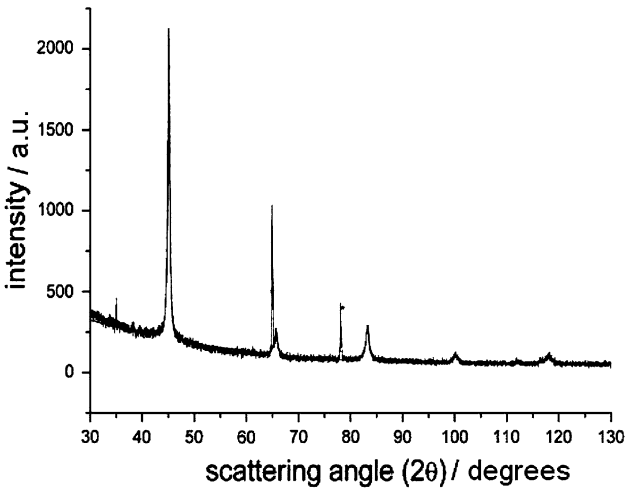

Fig. 7 XRD pattern of Co–Fe nanopowders

4 Conclusions

The production of $Co_{65}Fe_{35}$ alloy nanoparticles from Aotani solutions in the presence of high power ultrasound (20 kHz) is a simple and inexpensive technique. From potentiostatic and galvanodynamic studies, it was shown that: (i) sonication increases the efficiency of the electrodeposition process due to the increased movement of cations across the diffusion layer leading to a decrease in the overpotential; (ii) the limiting currents of iron and cobalt ions are different, but if the process is carried out under 'diffusion control' the composition of the produced nanoparticles is similar to that of the solution; (iii) the faradaic yield is mainly affected by both the current density and the time management; in fact, shorter current pulses and lower current densities increase the process efficiency. The morphological and structural studies showed that no individual Fe and Co metallic nanoparticles were produced sonoelectrochemically. The smallest particles had a mean dimension of about 5 nm, exhibited a *bcc* structure and were strongly aggregated in three-dimensional clusters of about 300 nm. This suggests that the sonoelectrochemical method produces nanoparticles of CoFe alloy which, due to their magnetic and high surface area properties, aggregate during the periods of aging in suspension and in filtration.

Acknowledgement The authors thank the European Community Sixth Framework Program through a STREP grant to the SELECT-NANO Consortium, Contract No. 516922.03/25/2005.

References

1. Mason TJ, Lorimer JP, Walton DJ (1990) Ultrason 28:333
2. Pollet BG, Phull SS (2001) In: Recent research developments in electrochemistry, chapt 4. Transworld Research Network Publisher, India, p 55
3. Viennet R, Ligier V, Hihn J-Y, Bereiziat D, Nika P, Doche M-L (2004) Ultrason Sonochem 11(3–4):125
4. Lorimer JP, Pollet B, Phull SS, Mason TJ, Walton DJ (1998) Electrochim Acta 43:449
5. Pollet BG, Hihn J-Y, Doche M-L, Lorimer JP, Mandroyan A, Mason TJ (2007) J Electrochem Soc 154(10):E131
6. Bai ZG, Yu DP, Wang JJ, Zou YH, Qian W, Fu JS, Feng SQ, Xu J, You LP (2000) Mater Sci Eng B72:117
7. Gedanken A (2004) Ultrason Sonochem 11:47
8. Qiu J-M, Bai J, Wang J-P (2006) Appl Phys Lett 89(22):222506/1
9. Ashassi-Sorkhabi H, Ghalebsaz-Jeddi N (2006) Ultrason Sonochem 13(2):180
10. Morales AM, Lieber CM (1998) Science 279(5348):208
11. Li SY, Lee CY, Tseng TY (2003) J Cryst Growth 247(3–4):357
12. Zhan Y, Zheng C, Liu YK, Wang G (2003) Mater Lett 57:3265
13. Chiorino A, Ghiotti G, Prinetto F, Carotta MC, Gnani D, Martinelli G (1999) Sens Actuator B Chem 58(1–3):338
14. Reisse J, Francois H, Vandercammen J, Fabre O, Kirsch-de Mesmaeker A, Maerschalk C, Delplancke JL (1994) Electrochim Acta 39(1):37
15. Suslick KS, Price GJ (1999) Annu Rev Mater Soc 29:295
16. Delplancke JL, Dille J, Reisse J, Long GJ, Mohan A, Grandjean F (2000) Chem Mater 12:946
17. Xu C, Xu G, Liu Y, Zhao X, Wang G (2002) Scripta Mater 46:789
18. Zhou H, Cai W, Zhand L (1999) Mater Res Bull 34:845
19. Lee ST, Wang N, Lee CS (2000) Mater Sci Eng A286(1):16
20. Guzman M, Delplancke JL, Long GJ, Delwiche J, Hubin-Franskin MJ, Grandjean F (2002) J Appl Phys 92:2634
21. Mancier V, Delplancke JL, Delwiche J, Hubin-Franskin MJ, Piquer C, Rebbouh L, Grandjean F (2004) J Magn Magn Mater 281:27
22. Jiang LP, Wang AN, Zhao Y, Zhang JR, Zhu JJ (2004) Inorg Chem Commun 7:506
23. Reisse J, Caulier T, Deckerkheer C, Fabre O, Vandercammen J, Delplancke JL, Winand R (1996) Ultrason Sonochem 3:S147
24. Delplancke JL, Bouesnard O, Reisse J, Winand R (1997) Mater Soc Symp Proc 451:383
25. Debouttiere P-J, Roux S, Vocanson F, Billotey C, Beuf O, Favre-Reguillon A, Lin Y, Pellet-Rostaing S, Lamartine R, Perriat P, Tillement O (2006) Adv Funct Mater 16(18):2330
26. Delplancke JL (2003) In: Baraton M-I (ed) Synthesis, functionalization and surface treatment of nanoparticles. American Scientific Publisher, California
27. Pollet BG, Lorimer JP, Hihn J-Y, Phull SS, Mason TJ, Walton DJ (2002) Ultrason Sonochem 9:267
28. Jones DA (1992) Principles and prevention of corrosion. Macmillan Publishing Company, New York
29. Brenner A (1963) Electrodeposition of alloys: principles and practices. Academic Press, New York
30. Aotani K (1952) J Electrochem Soc Jpn 20:31
31. Kim D, Park D-Y, Yoo BY, Sumodjo PTA, Myung NV (2003) Electrochim Acta 48:819
32. Margulis MA, Malt'sev AN (1969) Russ J Phys Chem (Transl Khim Zh Fiz) 43:1055
33. Margulis MA, Margulis IM (2003) Ultrason Sonochem 10:343
34. Correira AN, De Oliveira RCB, De Lima-Neto P (2006) J Braz Chem Soc 17(1):90
35. Sasaki KJ, Talbot JB (1995) J Electrochem Soc 142(3):775
36. Nurmi JT, Tratnyek PG, Sarathy V, Baer DR, Amonette JE, Pecher K, Wang C, Linehan JC, Matson DW, Penn RL, Driessen MD (2005) Environ Sci Technol 39(5):1221
37. Young RA (1993) The rietveld method. Oxford University Press, Oxford
38. Smithells CJ (1962) Metal reference book, vol 1. Butterworths, London